Effects of doping, electron irradiation, H^+ and He^+ implantation on the thermoelectric properties of Bi_2Se_3 single crystals

2005 J. Phys.: Condens. Matter 17 2873

(http://iopscience.iop.org/0953-8984/17/19/005)

INSTITUTE OF PHYSICS PUBLISHING JOURNAL OF PHYSICS: CONDENSED MATTER

J. Phys.: Condens. Matter **17** (2005) 2873–2888 doi:10.1088/0953-8984/17/19/005

Effects of doping, electron irradiation, H^+ and He^+ implantation on the thermoelectric properties of Bi_2Se_3 single crystals

Augustine Saji[1,2,3], S Ampili[1], Seong-Ho Yang[2], Kang Jeung Ku[2] and Mathai Elizabeth[1]

[1] Crystal Growth Laboratory, Department of Physics, Cochin University of Science and Technology, Cochin-682022, Kerala, India
[2] Materials and Process Simulation Laboratory, Department of Materials Science and Engineering, Korea Advanced Institute of Science and Technology (KAIST), Daejeon 305701, Republic of Korea

E-mail: sajia@kaist.ac.kr

Received 5 December 2004, in final form 24 March 2005
Published 29 April 2005
Online at stacks.iop.org/JPhysCM/17/2873

Abstract

As-grown single crystals of Bi_2Se_3 are doped with varying percentages of tellurium. These crystals are irradiated and implanted with electrons of energy 8 MeV and H^+ and He^+ ions of energy 1.26 MeV for comparative studies on their properties. Effects on the thermoelectric properties of Bi_2Se_3 due to high-energy electron bombardment (8 MeV), H^+ and He^+ ion implantation and doping are studied at temperatures ranging from 150 to 380 K. Crystal homogeneity and surface dislocations are determined using EDAX and SEM. Hot-probe and Hall effect measurements show that as-grown, electron irradiated and ion implanted crystals are n-type. Thermal diffusivity measurements prove the effective scattering mechanism (phonons) in Bi_2Se_3 crystals and provide a valid reason for reduced thermo-power in doped crystals.

1. Introduction

Thermoelectric materials are recently attracting renewed interest because of their potential applications in solid state thermoelectric cooling and electrical power generation devices [1, 2]. These thermoelectric (TE) devices have a wide variety of applications from cooling devices for seats in luxury automobiles to power supplies for spacer craft [3]. They have many attractive features compared with other methods of refrigeration or electric power generation, such as long life, no moving parts, no emission of toxic gases, low maintenance and high reliability [4].

[3] Author to whom any correspondence should be addressed.

Hence a broad and intense search has been underway to identify new materials with enhanced thermoelectric properties [5–8]. Recently, Venkatasubramanian *et al* [1] and Harman *et al* [4] have reported exciting high room temperature figures of merit (ZT) of 2.4 and 1.3 respectively in devices made out of nanostructures of conventional TE materials.

Conventional TE cooling materials are bulk solid solution alloys of Bi_2Te_3, Bi_2Se_3 and Sb_2Te_3 with the best materials having room temperature ZT values of 1.0 [9]. So far most investigations are focused on tuning the composition of these alloys and doping with other heavy metals [10–12]. Several classes of materials are currently under investigation including skutterudites, half-Heusler alloys, clathrates and pentatellurides [13–16]. Yet the vision of widespread use of thermoelectric energy conversion devices has remained elusive.

Even though bismuth selenide is not as technologically important as bismuth telluride, solid solutions of Bi_2Se_3 with Bi_2Te_3 are well known thermoelectric cooling materials. Bi_2Se_3 is properly crystallizable under controlled conditions and easily cleavable. Hence it could be considered as a model compound among thermoelectric materials for both experimental and theoretical analysis. Bismuth selenide belongs to a class of narrow bandgap layered semiconductors with tetradymite structure having space group $R\bar{3}m$–D^5_{3d}. Physical properties establishing Bi_2Se_3 as a semiconductor were studied earlier [17–20]. We have reported the growth, morphology, hardness and thermal diffusivity of Bi_2Se_3 single crystals and the effects of Te doping on these properties [21, 22]. Review articles and data sheets are available on the electrical, optical and galvanomagnetic properties of Bi_2Se_3 by various researchers [23–26]. There are also many reports regarding the underlying band structure and the nature of charge carrier scattering mechanisms in these crystals [27–29]. Even though a large volume of work has been done on the thermoelectric and optical properties of Bi_2Se_3 single crystals, there is no literature available on ion implantation and electron irradiation on these crystals other than the work done by Kar'kin *et al* on Bi_2Te_3 [30, 31].

The basic disadvantage of the TE compounds like Bi_2Se_3 is that they are not well defined, highly composition dependent and not as efficient as the device needs to be. Moreover, both the efficiency and coefficient of performance of a TE device are directly related to the figure of merit

$$Z = \frac{\alpha^2 \times \sigma}{\kappa} \tag{1}$$

where α is the thermo-power, σ is the electrical conductivity and κ is the thermal conductivity of the system. Hence, to improve the figure of merit one must think of ways and means to increase the value of $\alpha^2\sigma$ and decrease the thermal conductivity. Since these properties are determined by the details of electronic structure (bandgap, band shape, band degeneracy near the Fermi level) and scattering of charge carriers, they are not independent of each other. Hence we tried to introduce defects artificially, considering that the creation of defects in the material may enhance the electrical conductivity and hence the figure of merit also. In the present paper, we report the effects of electron bombardment, proton and He^+ ion implantation on Bi_2Se_3 single crystals. We also compare the characteristic properties of Bi_2Se_3 crystals after doping, electron irradiation and ion implantation.

2. Experimental details

Single crystals of Bi_2Se_3 and its Te doped samples are prepared from 5 N pure Bi, Se and Te. The synthesis of the compounds is carried out in tapered quartz ampoules evacuated to a pressure of 10^{-5} Torr. The sealed ampoules containing the charge are kept in a muffle

furnace having a flat temperature profile at 600 °C for 24 h. The ampoule is rotated and rocked periodically to ensure complete mixing and reaction. The compounds are identified using a Rigaku x-ray diffractometer with monochromatic nickel filtered Cu Kα radiation as the x-ray source. The powder diffractogram reveals the formation of Bi_2Se_3 and Bi_2Se_3 with varying concentrations of Te. The crystals are grown using the vertical normal freezing (VNF) method and it is possible to obtain single crystals of good quality by this method. The ampoule containing the melt is heat treated at 720 °C for 24 h and then moved at the rate of 4 mm h^{-1} through a temperature gradient of about 10 °C cm^{-1}. Single crystals 50 mm long and 8 mm in diameter are obtained by this method.

The crystals thus grown have (111) cleavage planes aligned parallel to the growth direction. Specimens from the middle portion of the as-grown crystals of dimension $12 \times 5 \times 0.3$ mm^3 are cut along the growth direction and used for electron irradiation. The samples are well packed in a polythene cover and kept in front of the Microtron output at a distance of 30 cm in open air. The samples are irradiated with electrons of energy 8 MeV for different fluences of the order 10^{15}–10^{17} cm^{-2}.

Single crystals of thickness approximately about 0.2–0.3 mm are used for the implantation of 1.26 MeV H^+ and He^+ ions (implantation energy is calculated from the SRIM programme). Different fluences of the order of 10^{14}–10^{15} ions cm^{-2} are implanted into these samples by keeping it in a high vacuum chamber maintained at 10^{-8} Torr. The ion beam is focused to a spot size of 1 mm^2 and scanned over an area of 10 mm $\times$ 10 mm using a fluorescent tape to irradiate the sample uniformly. The fluence is measured by collecting the charge falling on the sample mounted on a ladder placed in a secondary electron-suppressed geometry. The ladder current is integrated with a digital current integrator and charge pulses are counted. The charge pulses produced are directly proportional to the number of H^+ and He^+ ions bombarding the sample.

The electrical conductivity is measured parallel to the growth axis by the two-point probe method and the Hall coefficient is determined by the Van der Pauw technique. The accuracy of the electrical conductivity measurements by the two-point probe method is verified by the Van der Pauw technique. In order to reduce the error introduced by voltages from Seebeck and Peltier effects, the current is limited to 1–5 mA and the applied magnetic field is 5000 G. The Seebeck coefficient of the as-grown crystals is determined by measuring the voltage and temperature difference across the sample. A chromel–alumel thermocouple has been used as the measuring probe for the voltage difference across the sample. (Instruments used: Keithley nanovoltmeter model 181, Keithley model 195 DMM.) Mathematical equations used to find different experimental parameters are shown elsewhere [32].

Thermal diffusivity measurements are carried out using the photo-acoustic (PA) technique in the heat transmission configuration, also known as the open photo-acoustic cell (OPC) technique. A schematic diagram of the experimental set-up is shown in figure 1. The minimal volume OPC configuration gives a large signal to noise ratio compared to the conventional photo-acoustic cell. The sample is fixed to the top of the air chamber of the OPC using vacuum grease and it is irradiated on the surface facing the ambient. Continuous wave laser radiation at 488 nm from an argon ion laser is used as the source of optical excitation. The laser beam, which has $1/e^2$ radius of 0.6 mm, is used without further focusing so as to avoid lateral diffusion. Laser radiation with a power level at 50 ± 0.25 mW intensity is modulated using a mechanical chopper (Stanford Research Systems SR 540) before it falls on the specimen. The pressure fluctuations created in the acoustic chamber are detected by a sensitive microphone (Knowles BT 1754). The output of the microphone, which has a built in preamplifier, is fed to a dual-channel digital lock-in amplifier (Stanford Research Systems SR 830).

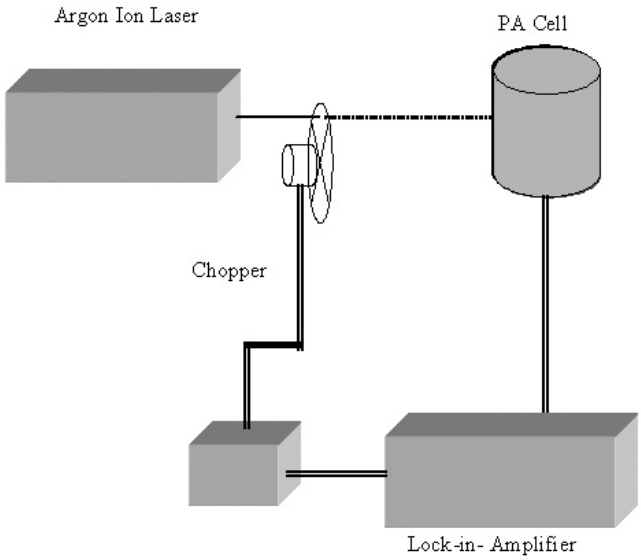

Figure 1. A schematic diagram of the photo-acoustic cell.

Table 1. Elemental atomic wt% (EDAX) of Bi_2Se_3, $Bi_2Se_{2.95}Te_{0.05}$, $Bi_2Se_{2.9}Te_{0.1}$ and $Bi_2Se_{2.7}Te_{0.3}$ single crystals.

	Actual atomic wt% (calculated)			Experimental atomic wt% (EDAX)		
Name	Bi	Se	Te	Bi	Se	Te
Bi_2Se_3	40	60	—	45	55	—
$Bi_2Se_{2.95}Te_{0.05}$	40	59	01	—	—	—
$Bi_2Se_{2.9}Te_{0.1}$	40	58	02	42	55.5	2.5
$Bi_2Se_{2.7}Te_{0.3}$	40	54	06	45	50	05

3. Results and discussion

3.1. Compositional analysis

Compositional analysis and crystal homogeneity are verified by powder x-ray analysis and energy dispersive x-ray analysis (EDAX). The x-ray diffractogram with sharp peaks indicates the crystallinity of these compounds. The results are compared with standard values given in JCPDS file no 12-732 and are found to agree very well with the standard values. Hence the stoichiometric compound formation of Bi_2Se_3 is confirmed.

To verify the stoichiometric deviation from the actual atomic wt%, the EDAX spectrum is taken for different regions of the single crystals. It is found that there are deviations from stoichiometry in varying degrees in most of the single-crystal regions selected for recording the spectrum. Table 1 gives the average value of actual (calculated) atomic wt% with experimentally observed atomic wt% from the middle portion of the crystal with an experimental error of $\pm 2\%$. EDAX results show that there is excess Bi and deficiency of Se or Te in all the as-grown crystals, but these deviations are within the expected limit of the experiment.

Dislocation density is determined to know the usability of the surface for further studies. Dislocation density is found to be of the order of 10^3–10^4 cm^{-2}. Powder x-ray diffractogram,

dislocation density (not exceeding 10^4) and EDAX [21] results prove that the as-studied regions of single crystals are more fairly stoichiometric and good to use for the present work.

3.2. SRIM calculations

Ion implantation is considered to be a uniform distribution of elements compared to conventional doping. The electronic and nuclear energy loss in the case of H^+ and He^+ ions increases to a maximum value (electronic loss is maximum at 80 keV for H^+ and 700 keV for He^+; nuclear loss is maximum at 10 keV for both) as the ion beam energy increases and thereafter decreases until 1 GeV. The maximum electronic energy loss in Bi_2Se_3 is 0.1848 eV $Å^{-1}$ for H^+ and 0.5088 eV $Å^{-1}$ for He^+ ions, while the maximum nuclear energy loss is 0.0012 and 0.001 08 eV $Å^{-1}$ for H^+ and He^+ ions respectively. The ion beam penetration range in Bi_2Se_3 single crystals shows a linear increase with the ion beam energy in both cases. The projected range for H^+ and He^+ ions of 1.26 MeV are 15.78 and 3.66 μm respectively. Since the calculated range of damage is around 4–15 μm, single crystals beyond the damage range will be initially unaffected by the displacement process due to implantation. However defect transport into these regions may occur. It is assumed that the ions penetrating into the target are implanted inside since the range of 1.26 MeV is less than the thickness of the sample.

3.3. Type of conductivity

Hot probe and Hall effect measurements have shown that as-grown crystals (Bi_2Se_3 and its various percentages of Te doped single crystals) are n-type. Electron irradiation or ion implantation does not have any effect on the type of conductivity. All these crystals remain as n-type conductor even after the electron bombardment and ion implantation.

The free carrier concentration in n-type Bi_2Se_3 is approximately given by the relation

$$[e] = [V^{\bullet}_{Se}] - [Bi'_{Se}]. \tag{2}$$

Hence the electronic conductivity of Bi_2Se_3 can be well explained by the probable formation of the positively charged selenium vacancies $[V^{\bullet}_{Se}]$ and antisite (AS) defects like bismuth atoms in selenium sites $[Bi'_{Se}]$ [33, 34]. Moreover, the formation of antisite defects $[Bi'_{Se}]$ does not alter the bonding structure of Bi_2Se_3 [35]. In addition to the above circumstantial evidence of antistructure formation and the corresponding n-type conductivity, there is substantial proof given by various authors for the n-type conductivity of Bi rich Bi_2Se_3 [34–36, 23] single crystals. Hence the as-grown crystals of Bi_2Se_3 and its Te doped crystals naturally become n-type conductors since they are super-stoichiometric in Bi as evidenced from EDAX and proved by hot probe and Hall effect measurements.

3.4. Comparison of electrical conductivity due to Te doping

Incorporation of Te atoms into Bi_2Se_3 crystal lattice results in a marked increase in the absolute value of σ in the extrinsic conduction region as shown in figure 2. Also in the intrinsic conduction region, the absolute value of σ is a maximum for pure Bi_2Se_3 single crystals. Electrical conductivity monotonically decreases with temperature and shows a pronounced minimum near 300 K for undoped Bi_2Se_3 single crystals and 340–350 K for doped crystals. Thereafter, the conductivity increases as the temperature increases. The temperature corresponding to σ_{min} shifts towards the higher temperature region as the doping concentration is increased. Hence Bi_2Se_3 and its Te doped single crystals show metallic conductivity in the 150–340 K range and semiconducting behaviour for temperatures above 340 K. Carrier density shows similar variations to that of electrical conductivity in the extrinsic and intrinsic

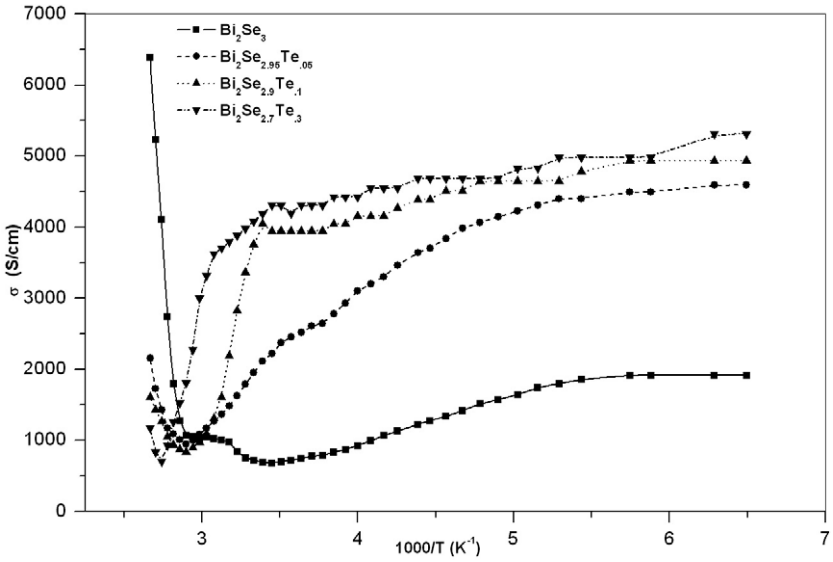

Figure 2. Plot of σ versus $(1000/T)$ for Bi_2Se_3 and its Te doped single crystals.

conduction region for the as-grown single crystals. Hence these conductivity variations are very well supported by the temperature dependence of the carrier concentration as in figure 3.

The above observed effect could be explained when we take into account the possibility of formation of uncharged substitutional defects (Te^{*}_{Se}), selenium vacancies ($V^{\bullet}_{Se}$), anti-structural defects like (AS) (Bi'_{Se}), bismuth at interstitial positions (Bi_i) and also inclusion of Bi at the van der Waals gap. Even though there are possibilities of formation of antisite defects like Se'_{Bi} and Te'_{Bi}, these could be discarded due to deficiency of Se and Te in Bi_2Se_3 from the experimental evidence of EDAX. Hence the formation of selenium vacancies ($V^{\bullet}_{Se}$) is also accounted for. Since Bi is super-stoichiometric in the as-grown crystals, there is every possibility of formation of AS defects such as Bi'_{Se}. If these defects are more numerous compared to the $V^{\bullet}_{Se}$, then there should be substantial reduction in the concentration of free electrons according to equation (2). Instead, conductivity and carrier density increases for higher tellurium content. Hence it could be assumed that formation of anti-structural defects (Bi'_{Se}) are suppressed. This may be due to the uncharged, negatively polarized Te^{*}_{Se} defects. Defects like Te^{*}_{Se} produce higher polarization in bonds between the defect and the neighbouring Bi atoms in comparison with the Bi–Se bonds. Hence a small negative charge (δ^{-}) originates from the defect of Te^{*}_{Se} which contributes bond ionicity. Therefore an increase in the Te content in the crystal lattice of Bi_2Se_3 could increase the bond polarization, which eventually suppresses the antisite defects. This could be one of the reasons for the increase in electrical conductivity with the simultaneous increase of carrier density. These assumptions are based on the facts put forward by Krebs, Horak and Novotny [37–39].

The other possible reasons for the above experimental observations are the interstitial and intercalation effects in the van der Waals gap. The addition of Te atoms to the Bi_2Se_3 lattice results in a measurable increase in the values of lattice parameters of pure Bi_2Se_3 and is shown in table 2. But the ratio of c/a remains virtually constant, of the order of 6.92, like that of pure Bi_2Se_3. The very fact that the ratio of c/a does not change leads us to the conclusion of a preferable formation of interstitial defects within the layers. In the case of doping of Te atoms in the van der Waals gap, we would suppose a deformation of the crystal lattice and

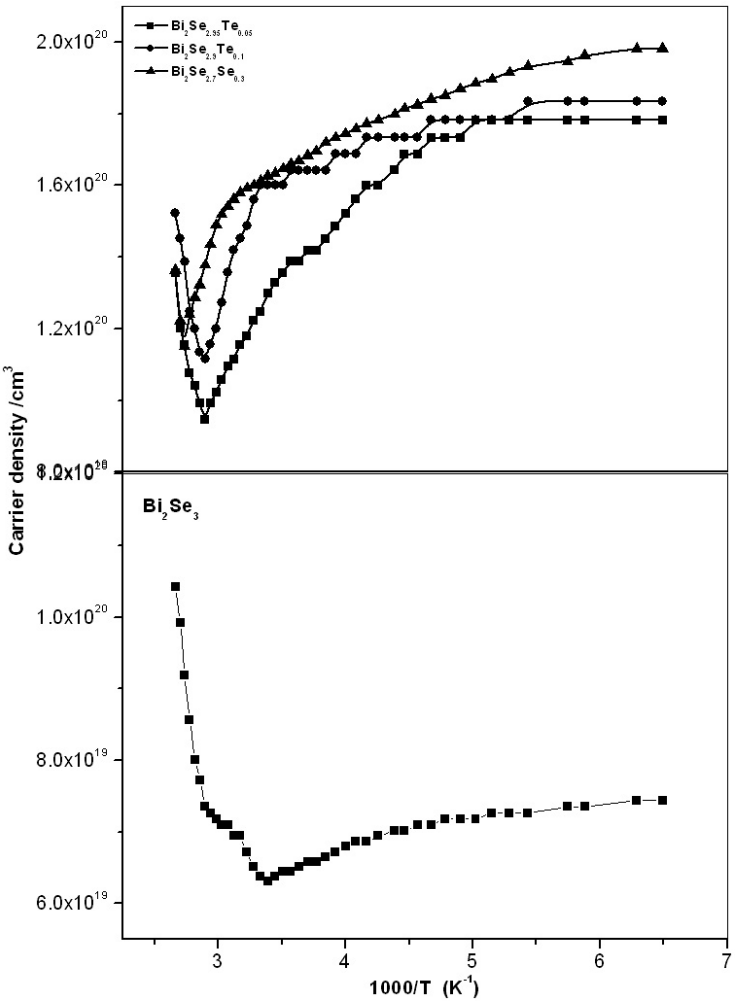

Figure 3. Carrier density as a function of inverse temperature for Bi_2Se_3 and its Te doped single crystals obtained from the Hall coefficient.

hence a change in the c/a ratio. Since this has not been observed, Bi_i and Te_i are supposed to be the other reasons for the enhancement in free electrons and conductivity. Further, there is a very acceptable idea that because of the relatively high permittivity of the Bi_2Se_3 lattice ($\varepsilon_\infty = 29$) bismuth and tellurium atoms at interstitial sites are ionized, providing electrons to the conduction band so that free electron concentration considerably increases.

3.5. Comparison of electrical conductivity due to irradiation and implantation

Electron irradiated, H^+ and He^+ ion implanted crystals show an increase in absolute value of electrical conductivity as in figure 4. As we study the conductivity variations with temperature, electron irradiated Bi_2Se_3 single crystals start showing semiconducting nature in the range 300–325 K, 350–365 K for H^+ and 340–350 K for He^+ implanted crystals. Moreover, the electrical conductivities of H^+ and He^+ ion implanted crystals remain constant up to 320 K. Above 320 K, the conductivity decreases to a minimum value and then increases. Table 3 presents the

Table 2. Calculated lattice parameter values, thermal diffusivity (α_{max}), and $\alpha^2\sigma_{max}$ for as-grown and Te doped Bi_2Se_3 single crystals.

	Standard value of lattice parameter from JCPDF			Calculated value of lattice parameter					
Samples	a (Å)	c (Å)	c/a	a (Å)	c (Å)	c/a	Thermal diffusivity ($cm^2\ s^{-1}$)	α_{max} (μ_V/K)	$\alpha^2\sigma_{max}$ (W cm^{-1} K^2)
Bi_2Se_3	4.133	28.62	6.92	4.134	28.68	6.93	0.312 ± 0.002	261	3.496×10^{-6}
$Bi_2Se_{2.95}Te_{.05}$	—	—		4.139	28.63	6.91	0.070 ± 0.001	245	3.968×10^{-6}
$Bi_2Se_{2.9}Te_{0.1}$	—	—		4.143	28.68	6.92	0.077 ± 0.002	202	5.471×10^{-6}
$Bi_2Se_{2.7}Te_{0.3}$	—	—		4.166	28.83	6.92	0.090 ± 0.003	124	2.074×10^{-6}

Table 3. Transition temperature and activation energy values for Bi_2Se_3 crystals.

Samples	Transition temp. (K) (T for σ_{min})	Activation energy (E_a) eV	Fluences (cm^{-2})
Bi_2Se_3	300	0.32	—
e5	295	0.37	4.098×10^{15}
e10	305	0.34	8.197×10^{15}
e15	325	0.41	1.229×10^{16}
e125	335	0.44	1.024×10^{17}
H^+	350	0.45	1×10^{14}
H^+	360	0.65	5×10^{14}
H^+	365	0.53	1×10^{15}
He^+	345	0.52	1×10^{14}
He^+	340	0.48	5×10^{14}
He^+	350	0.57	1×10^{15}
$Bi_2Se_{2.95}Te_{0.05}$	345	0.35	—
$Bi_2Se_{2.9}Te_{0.1}$	345	0.32	—
$Bi_2Se_{2.7}Te_{0.3}$	365	0.60	—

transition temperature values from metallic to semiconducting character for different fluences and doping. The increase in absolute value of electrical conductivity of electron irradiated and ion implanted crystals compared to undoped ones is interrelated with the numbers of carriers taking part in the conduction. Figure 5 clearly shows the enhancement in electrical conductivity due to the substantial increase in electron concentration by irradiation and implantation.

Radiation induced defects might have been created when Bi_2Se_3 single crystals are bombarded with 8 MeV electrons. So it would be better assumed that interstitial defects like Bi_i are formed during electron irradiation along with AS defects and vacancy formation. Moreover, these interstitial defects might have been ionized and provide free electrons for the conduction mechanism. Hence it could be concluded that the increase in the absolute value of electrical conductivity will be due to the ionized interstitial defects [Bi_i].

When compared to electrons, high energy H^+ and He^+ ions lose energy at a much higher rate. For high proton and He^+ energies, the particles mainly cause ionization. For lower energies, collisions with lattice atoms become more important. As a consequence of their higher mass with respect to electrons, protons can transfer more energy in an elastic collision onto lattice atoms. For 1.26 MeV H^+ and He^+ ions, the stopping range varies approximately from 4 to 16 μm from SRIM calculations. Hence these ions are effectively doped and produce defects in the crystal lattice.

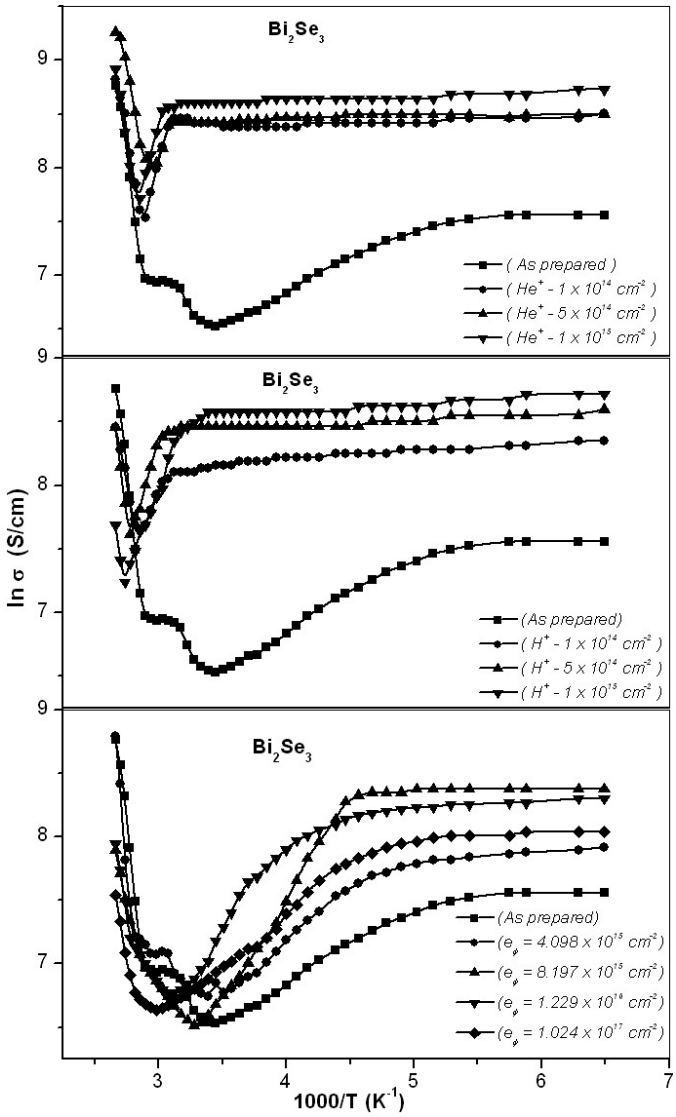

Figure 4. Plot of $\ln\sigma$ versus $(10^3/T)$ for electron irradiated, H^+ and He^+ ion implanted Bi_2Se_3 single crystals.

Woodhouse *et al* have reported the decrease in resistivity by proton bombardment on InP structures [40]. From the experimental results of H^+ and He^+ ion implantation on Bi_2Se_3 (figure 4), conductivity increases with respect to the undoped sample. Hence it would be reasonable to assume that principal effects of implantation are to introduce defects that act as donors. Above a certain threshold energy for the incident particle (electron, proton and He^+ ions), Frenkel pairs are generated in the solid. Depending on the respective temperature and the position of the interstitials, the Frenkel pairs can spontaneously recombine or form permanent defects like point defects or clusters in the crystal lattice [41]. These defects might have been ionized and the effective value of the conductivity could increase as the number of carrier increases.

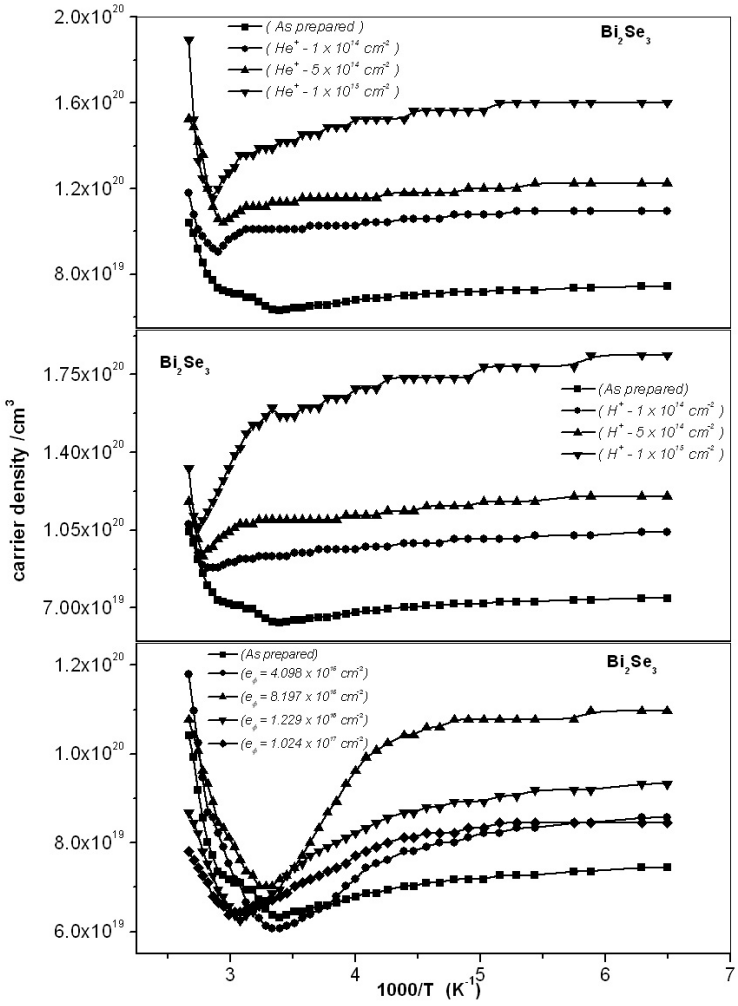

Figure 5. Carrier density as a function of inverse temperature for electron irradiated H^+ and He^+ ion Bi_2Se_3 single crystals obtained from Hall coefficient.

Table 3 provides the comparison of activation energy for undoped, doped, electron irradiated, H^+ and He^+ ion implanted Bi_2Se_3 single crystals determined from conductivity studies using the equation

$$\sigma = \sigma_0 \exp\left(\frac{-E_a}{k_B T}\right) \tag{3}$$

where σ is the absolute value of conductivity, E_a is the activation energy, k_B is the Boltzmann constant and T is the temperature.

3.6. Dependence of Hall coefficient (R_H) and mobility (μ_H) on temperature

Hall coefficient and mobility variations with inverse temperature are shown in figures 6 and 7. The Hall coefficient remains fairly constant up to the transition temperature shown in table 3; thereafter, it slowly decreases and starts increasing from a particular minimum value.

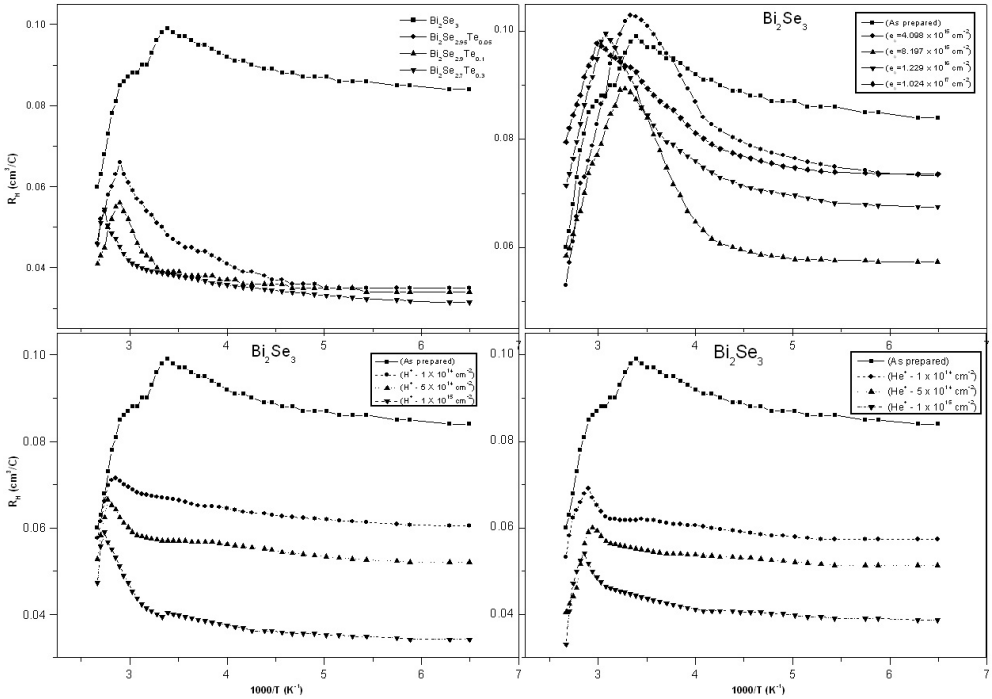

Figure 6. Hall coefficient as a function of inverse temperature for doped, electron irradiated, H^+ and He^+ ion implanted Bi_2Se_3 single crystals.

The absolute value of R_H is found to be decreasing as the doping concentration, dosage of electron irradiation or dosage of ion implantation is increased. The positive and negative slopes of R_H versus T and σ versus T itself prove the metallic to semiconducting behaviour of Bi_2Se_3. Undoped Bi_2Se_3 single crystals exhibit semiconducting nature from 300 K onwards. Doping, electron irradiation and ion implantation resulted in further increase of this value to 330–360 K. Hence it could be concluded that, even though the resistivities of these structures are enhanced, the semiconducting nature of the crystal is restored between 330 and 360 K by effective doping, high-energy electron irradiation and ion implantation. The negative value of R_H confirms the n-type conductivity of the crystals studied.

It is seen that mobility variations are similar to that of conductivity. Increase in μ_H depends on the doping percentage of Te, dosage of electron bombardment and ion implantation. But the mobility variations are not found to be too high. This again supports the conductivity variations as well as the conversion of metallic to semiconducting nature of Bi_2Se_3 single crystals. The power factor $m \cong 0.5$–1.3 (obtained from mobility variations with temperature) indicates that the transport mechanism is dominated by phonon scattering in Bi_2Se_3 and its Te doped single crystals. These findings are substantiated by the detailed thermal diffusivity studies explained below.

3.7. Comparative study of electronic thermal conductivity (K_{el})

Electronic contribution of thermal conductivity shows a noticeable increase in the case of doped, electron irradiated and ion implanted crystal samples of Bi_2Se_3 compared to the undoped one. There is significant enhancement in the value of K_{el} for higher Te content and

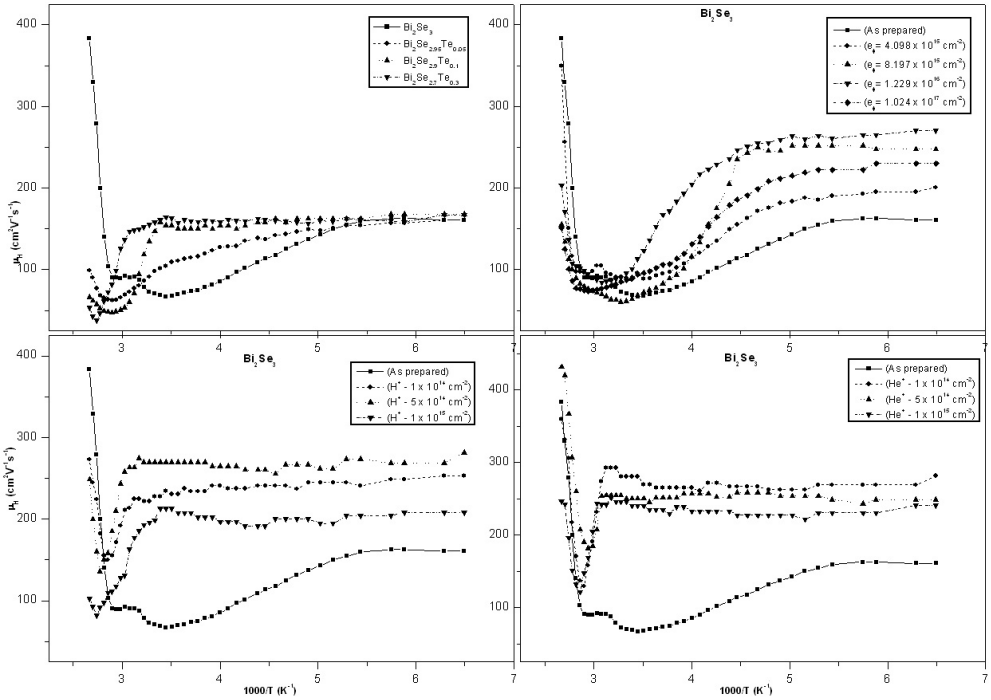

Figure 7. Plot of μ_H versus $(10^3/T)$ for doped, electron irradiated, H^+ and He^+ ion implanted Bi_2Se_3 single crystals.

an insignificant increase of K_{el} for higher doses of electron irradiation and ion implantation. It could be worth noting that K_{el} remains almost constant over a temperature range from 150 to 300 K and thereafter it decreases or increases depending on the metallic or semiconducting nature as shown in figure 8.

3.8. Dependence of thermal diffusivity and Seebeck coefficient (α) *on doping*

Thermal diffusivity and thermo-power variations for the doped samples are shown in table 2. Results show that both the parameters of the doped samples are less than that of the undoped one. We know that heat is essentially transported by phonons in crystals. So the value of thermal diffusivity depends directly on the phonon mean free path, which is governed by various phonon scattering processes occurring in the specimen. These scattering processes in the sample are affected by the nature of dopants and their concentration [42]. Hence the introduction of Te dopants into the Bi_2Se_3 lattice generates extra scattering centres for phonons. This results in reduction of the phonon mean free path and gives a reduced value for the thermal diffusivity, which also substantiates the thermo-power variations in the crystals. Thermo-power (Seebeck coefficient) depends on the effective number of thermal carriers reaching the colder zone. Most of the thermal carriers are scattered as we increase the doping concentration of Te and hence a reduced value for thermo-power is obtained.

Figure 9 shows the temperature dependence of thermo-power (α) and $\alpha^2\sigma$ for Bi_2Se_3 and its Te doped single crystals. With increasing temperature, the α and $\alpha^2\sigma$ graph has an asymmetric broadening near the intrinsic conduction regime. The maximum value of α shifts to higher temperatures and becomes broadened with increasing Te content. As we increase the doping percentage of Te, the absolute value of α decreases. Table 2 provides the maximum

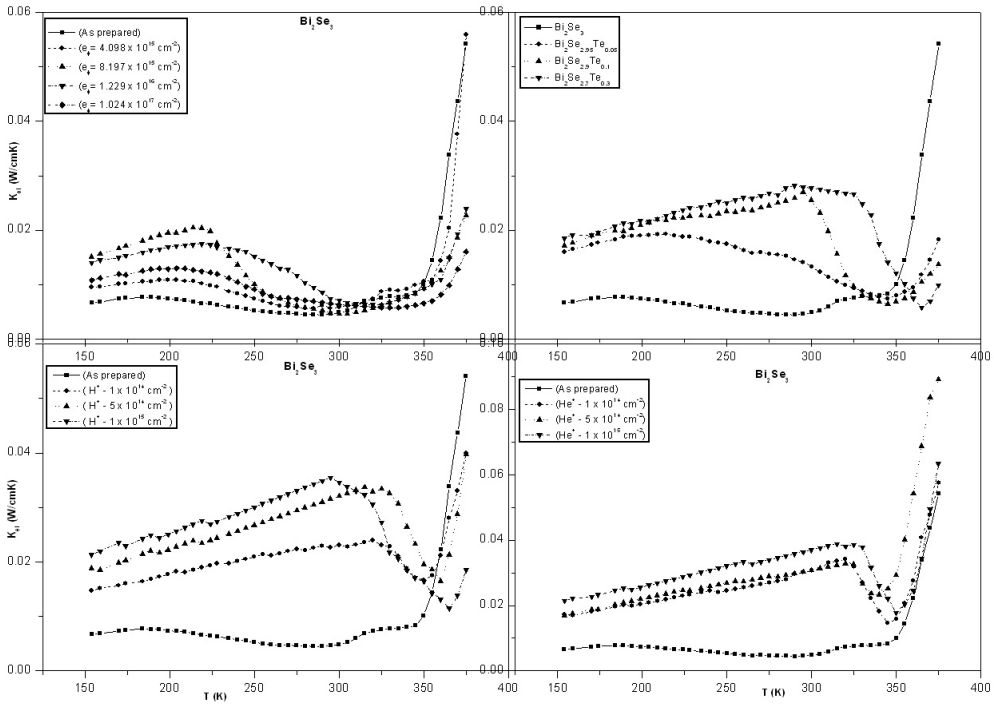

Figure 8. Temperature dependence of K_{el} for doped, electron irradiated, H^+ and He^+ ion implanted single crystals.

value of α and $\alpha^2\sigma$. There are similar reports about the decrease in absolute value of α as Bi_2Se_3 is doped with indium [43]. Moreover, the temperature dependence of the Seebeck coefficient depends on the variation of Fermi energy with temperature and is shown in figure 10.

In order to explain the non-monotonic variations in transport properties of Bi_2Se_3 with the increase in concentration of Te, we studied the crystal structure using x-ray diffraction. The values obtained for the lattice spacing for doped and undoped samples are given in table 2. It is seen that the lattice spacing (parameter a) varies from 4.134 Å for an undoped sample to 4.166 Å for the doped one. This expansion in lattice spacing could be attributed to the point defects in crystals. For the specific property of thermal diffusivity in Bi_2Se_3, inclusion of Te dopants reduces the thermal diffusivity substantially because of the increased scattering centres due to various defects. But among the doped systems, as the Te concentration increases, thermal diffusivity increases and attains a higher value for $Bi_2Se_{2.7}Te_{0.3}$ crystals due to the enhancement in lattice spacing, which in turn increases the phonon mean free path. Thermo-power (α_{max}) variations also show lower values compared with the undoped sample which could also be explained on the basis of defects in the system (which we have already discussed in section 3.4). Increased defects means a possible increase in the scattering centres, which eventually scatter the thermal carriers, and a reduced value of thermo-power could be observed as in table 2.

4. Conclusion

In conclusion, we have measured the temperature dependence on transport properties of Bi_2Se_3 single crystals. The absolute value of the electrical conductivity in Bi_2Se_3 single crystals could be increased by effective doping, electron irradiation and ion implantation (H^+ and He^+

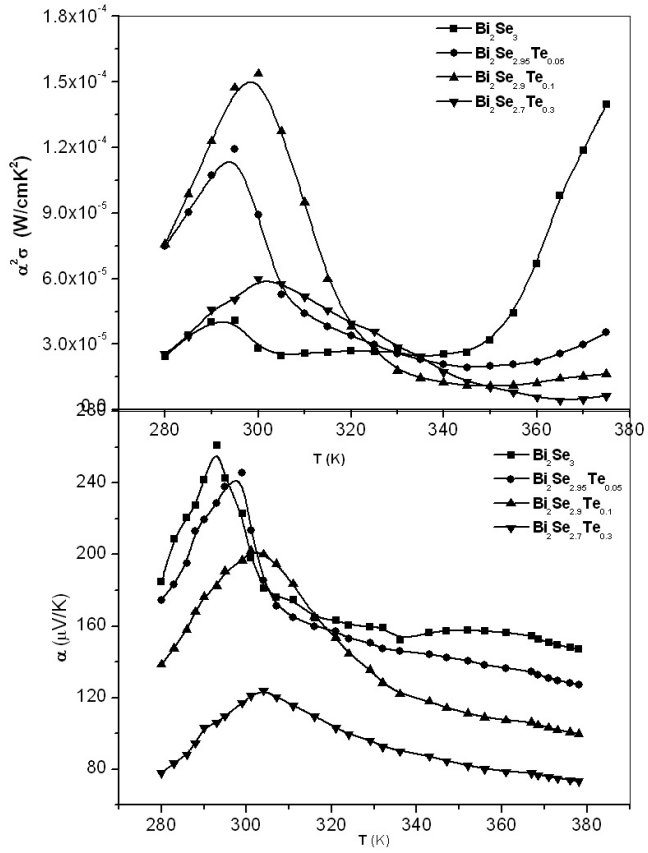

Figure 9. Temperature dependence of α, $\alpha^2\sigma$ for Bi_2Se_3 and Te doped single crystals.

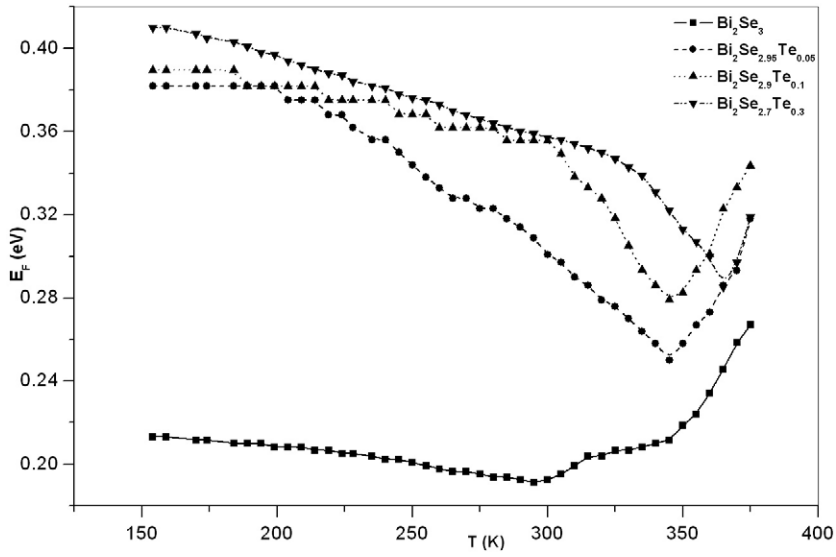

Figure 10. Temperature dependence of E_f for Bi_2Se_3 and Te doped single crystals.

ions). The substantial increase in the electrical conductivity by electron irradiation and ion implantation is due to the defects such as vacancies and interstitials created in the Bi_2Se_3 crystal lattice. Nuclear and electronic energy loss decrease as we increase the doping percentage of Te for both H^+ and He^+ ion implantation. All single crystals of Bi_2Se_3, whether it is doped with Te, electron irradiated or H^+ and He^+ ion implanted, are n-type semiconductors. Bi_2Se_3 shows semiconducting nature in the range of 300–360 K. Doping reduces the thermal diffusivity and thermo-power values of Bi_2Se_3 single crystals.

Acknowledgments

We would like to thank Professor Biju Raja Sekhar, IOP, Bhubaneswar, for providing the ion beam facility. Thanks to Professor Siddappa and Dr Ganesh of Mangalore University for providing the Microtron facility. Thanks to Professor Vikram Jayaram, IISc, Bangalore, for helping us with SEM and EDAX studies. Thanks to UGC for funding our department through DSA/COSIST scheme.

References

[1] Rama V, Siivola E, Colpitts T and O'Quinn B 2001 *Nature* **413** 597
[2] Jeffrey Snyder G, Lim J R, Huang C-K and Fleurial J P 2003 *Nat. Mater.* **2** 528
[3] Vining C B 2003 *Nature* **423** 391
[4] Harman T C, Taylor P J, Walsh M P and LaForge B E 2002 *Science* **297** 2229
[5] Hsu K F, Loo S, Guo F, Chen W, Dyck J S, Uher C, Hogan T, Polychroniadis E K and Kanatzidis M G 2004 *Science* **303** 818
[6] Chung D-Y, Hogan T, Brazis P, Rocci-Lane M, Kannewurf C, Bastea M, Uher C and Kanatzidis M G 2000 *Science* **287** 1024
[7] Disalvo F J 1999 *Science* **285** 703
[8] Lyeo H-K, Khajetoorians A A, Shi L, Pipe K P, Rajeev J R, Shakouri A and Shih C K 2004 *Science* **303** 816
[9] Rowe R M 1995 *CRC Handbook of Thermoelectrics* (Boca Raton, FL: CRC press)
[10] Borkowski K and Przyluski J 1987 *Mater. Res. Bull.* **22** 381
[11] Caillat T, Carle M, Pierrat P, Scherrer H and Scherrer S 1992 *J. Phys. Chem. Solids* **53** 1121
[12] Horak J, Cermak K and Koudelka L 1986 *J. Phys. Chem. Solids* **47** 805
[13] Sales B C, Mandrus D and Williams R K 1996 *Science* **272** 1325
[14] Uher C, Yang J, Hu S, Morelli D T and Meisner G P 1999 *Phys. Rev.* B **59** 8615
[15] Nolas G, Colin J L, Slack G and Schujman S B 1998 *Appl. Phys. Lett.* **73** 178
[16] Littleton R T, Tritt T M, Feger C R, Kolis J, Wilson M L, Marone M, Payne J, Verebeli D and Levy F 1998 *Appl. Phys. Lett.* **72** 2056
[17] Hashimoto K J 1970 *J. Phys. Soc. Japan* **16** 1961
[18] Koehler H and Landwehr G 1971 *Phys. Status Solidi* b **45** k109
[19] Koehler H and Becker C R 1974 *Phys. Status Solidi* b **61** 533
[20] Koehler H 1974 *Phys. Status Solidi* b **62** 57
[21] Saji A and Elizabeth M 2001 *Mater. Res. Bull.* **36** 2251
[22] George S D *et al* 2003 *Phys. Status Solidi* a **196** 384
[23] Stordeur M, Katavong K K, Priemuth A, Sobotta H and Ried V 1992 *Phys. Status Solidi* b **169** 505
[24] Mishra S K, Satpathy S and Jepsen O 1997 *J. Phys.: Condens. Matter* **9** 461
[25] Sklenar A, Drasar A, Krejcova A and Lostak P 2000 *Cryst. Res. Technol.* **35** 1069
[26] Woollam J A, Beale H A and Spain I L 1972 *Phys. Lett.* A **41** 319
[27] Navratil J, Horak J, Plechacer T, Kamba S, Lostak P, Dyck J S, Chen W and Uher C 2004 *J. Solid State Chem.* **177** 1704
[28] Larson P *et al* 2002 *Phys. Rev.* B **65** 85108
[29] Kulbachinski V A, Inoue M, Sasaki M, Negishi H, Gao W K, Takasa K, Lostak P and Horak J 1994 *Phys. Rev.* B **50** 16921
[30] Kar'kin A E, Shchennikov V V, Goshchitskii B N, Danilov S E and Abusov V L 1998 *J. Exp. Theor. Phys.* **86** 976

[31] Kar'kin A E, Shchennikov V V, Goshchitskii B N, Danilov S E, Abusov V L and Kulbachinski V A 2003 *Phys. Solid State* **45** 2249
[32] Saji A and Elizabeth M 2003 *Semicond. Sci. Technol.* **18** 745
[33] Horak J, Novotny R, Lostak P and Hoschl P 1987 *J. Phys. Chem. Solids* **48** 1227
[34] Horak J, Navratil J and Stray Z 1992 *J. Phys. Chem. Solids* **53** 1067
[35] Horak J, Stray Z, Lostak P and Pancir J 1990 *J. Phys. Chem. Solids* **51** 1353
[36] Hyde G R, Beale H A and Spain I L 1974 *J. Phys. Chem. Solids* **35** 1719
[37] Krebs H 1968 *Grundzuge der Anorganischen Kristall Chemie (Stutgart)* p 239
[38] Horak J, Lostak P and Benes L 1984 *Phil. Mag.* B **50** 665
[39] Novotny R, Lostak P and Horak J 1990 *Phys. Scr.* **42** 253
[40] Woodhouse J D, Donnelly J P and Iseler G W 1988 *Solid State Electron.* **31** 13
[41] Ulmaier H 1997 *Mater. Res. Bull.* **22** 14
[42] Castro Rodriguez R, Zapata Toress M, Rejon Moo V, Bartolo-perez P and Pena J L 1999 *J. Phys. D: Appl. Phys.* **32** 1194
[43] Jansa L, Lostak P, Sramkova J and Horak J 1992 *J. Mater. Sci.* **27** 6062